ACS Catalysis

pubs.acs.org/acscatalysis
Research Article

Energy Maps of Complex Catalyst Surfaces

Andrey V. Tarasov, Sabine Wrabetz, Jutta Kröhnert, Frank Rosowski, Robert Schlögl, and Annette Trunschke*

Cite This: ACS Catal. 2024, 14, 12581−12591
Read Online

ABSTRACT: Chemical reactions that are crucial for energy conversion require catalysts with intricate functional interfaces characterized by high structural and compositional complexity. Computational catalysis offers predictive insights through the simulation of surface structures and elementary processes, but reliable experimental benchmarks are essential for validation. In this study, we provide such experimental data by determining the energetic distribution of adsorption sites of short-chain alkanes (ethane, propane, *n*-butane) and alkenes (ethene, propene, 1-butene) on the surface of the polycrystalline oxides V_2O_5, $MnWO_4$, $SmMnO_3$, and $MoVO_x$, and on the benchmark catalyst vanadyl pyrophosphate $(VO)_2P_2O_7$ (VPP) using microcalorimetry. From the measurement of the heat of adsorption as a function of the degree of coverage, energy distribution spectra were derived, which represent a quantitative energetic fingerprint of the functional interface. Using the adsorption data, turnover frequencies were determined for the oxidation of propane, which served as a complex probe reaction. The integral heat of adsorption of the reactant propane normalized to the number of adsorption sites was thus determined as a descriptor for activity. Correlation diagrams of propane and propene adsorption allow to predict the selectivity. The maximum turnover frequency of the formation of valuable oxygenates is found at moderate adsorption strength of the intermediate propene. The presented method provides a reference data set for systems where detailed atomistic information about the structure of active sites is difficult to obtain due to their inherent complexity.

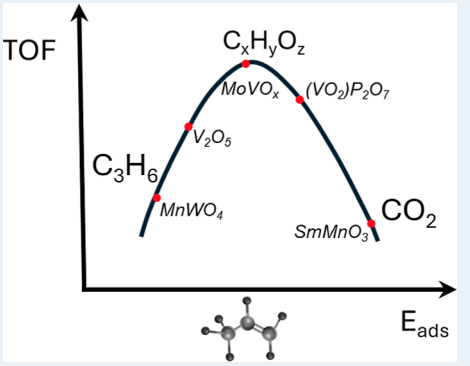

KEYWORDS: *microcalorimetry, propane adsorption, propene adsorption, adsorption sites, alkane oxidation*

INTRODUCTION

Adsorption at catalytically active interfaces allows chemical reactions to proceed more energy-efficiently than in the homogeneous phase since the reacting molecules are activated for alternative reaction pathways. The thermodynamics of adsorption processes are described by adsorption models, such as the widely used Langmuir adsorption isotherm. It is assumed that (i) an interaction takes place at identical adsorption sites via dispersion forces or the formation of chemical bonds, (ii) the heat of adsorption is constant regardless of surface coverage, and (iii) the adsorbed molecules do not interact with each other.[1] Microkinetic models frequently use the Langmuir adsorption isotherm to describe the kinetics of heterogeneously catalyzed reactions.[2,3] However, the validity of the above boundary conditions is rarely verified experimentally for exactly the catalyst systems whose kinetics is being studied.

The introduction of adsorption microcalorimetry[4,5] enabled the quantitative analysis of the heat of adsorption as a function of the degree of coverage on single crystals and powders and, thus, the characterization of the energetic distribution of adsorption sites on the surface of model systems and more complex catalysts.[6−9] Calorimetric measurements of the adsorption of probe molecules on oxides applied as heterogeneous catalysts show, in most cases, considerable energetic surface heterogeneity of the adsorption centers.[6] For the energetic distribution of Brønsted and Lewis acid sites in zeolites, so-called acidity strength spectra were recorded in the late 1970s.[10−12] Since then, no other solid catalyst has been studied similarly.

Microcalorimetry applied to characterize catalyst surfaces mainly involves the study of probe molecules, such as ammonia, SO_2 or CO. In rare cases, adsorbed reactants of relevant catalytic reactions are employed. In fact, there is essentially no information on the energetic distribution of adsorption sites on real high-performance catalysts.

Generally, the active sites on the surface of a heterogeneous catalyst are challenging to detect analytically. According to Taylor's concept,[13] only a small fraction of particularly coordinatively unsaturated surface atoms enables the activation of the adsorbed molecule for a reaction, and all other adsorption sites are resting places or sites for the adsorption

Received: March 1, 2024
Revised: July 24, 2024
Accepted: July 24, 2024
Published: August 7, 2024

https://doi.org/10.1021/acscatal.4c01308
ACS Catal. 2024, 14, 12581−12591

of spectator species. In complex reaction networks involving sequential and parallel chemical transformations, it cannot be excluded that several different active sites are involved in the overall pathway.[14] Detection is further complicated by the fact that the active state of a catalyst forms only under reaction conditions.[15,16] Thus, the determination of turnover frequencies (TOF),[17] which represent an absolute scale of catalytic activity in units of reacting molecules per active site per second, is a challenge in heterogeneous catalysis.

Computational heterogeneous catalysis generates key mechanistic insights and predicts improved catalysts.[18] However, this requires accurate quantification of the adsorption energies of major species involved in a reaction mechanism.[19] Explicit DFT calculations combined with a reduction of possible active surface structures of interest through machine learning techniques can accelerate progress in gaining insight.[20−22] Adsorption energies calculated by DFT, primarily derived for metals, reported values comparable with experiments.[8,23,24] However, atomistic information for complex catalyst surfaces and composites is lacking. Since the structure of the adsorption complex is unclear, computational studies that address oxides or other multicomponent systems can be subject to significant uncertainties.[25] But chemical reactions, which are essential for energy storage and conversion, usually require functional interfaces in catalyst materials with exactly this higher structural and compositional complexity.[26] Thus, the validity of energetic parameters used in the mechanistic analysis is critical when addressing the current challenges in catalysis research.[9,27] To tackle the complexity, systematic experiments on relevant high-performance multicomponent catalyst materials are needed, which may serve as benchmarks for theory.

In this work, we probe the adsorption energy distribution for C2−C4 alkanes and alkenes on metal oxides and phosphates, including V_2O_5,[28] $MnWO_4$,[29,30] $(VO)_2P_2O_7$,[28,31] $SmMnO_3$,[32,33] and $MoVO_x$,[34,35] and present a comprehensive data set for the interaction of alkanes and alkenes with oxide surfaces. The selection of materials focused on diversity in chemical composition and catalytic properties.[36,37] Alkane oxidation is an example of a highly complex type of reaction.[38,39] The industrial catalyst vanadyl pyrophosphate $(VO)_2P_2O_7$ (VPP) was included as a benchmark.[40] The nanostructure and surface composition of the compounds were previously investigated extensively by electron microscopy and synchrotron-based near-ambient-pressure photoelectron spectroscopy (NAP-XPS). Observed were phenomena such as surface elemental enrichment,[33,34] specific surface termination with an isolated group of atoms, point defects,[29] intergrowth of phases, segregation from channels, interstitial regions and inclination.[41] The cross-sectional area of the hydrocarbon molecules (0.1−0.5 nm^2) roughly corresponds to the dimensions of the surface irregularities (0.6−1.5 nm^2) detected by electron microscopy. Therefore, the adsorption experiments are expected to reflect well the energetic distribution of surface sites.

Since there is practically no data on the distribution of adsorption energies of reactants on the surface of complex catalysts, our research aims to fill this gap. By determining the energetic distribution of adsorption sites, data for the validation of models used in computational chemistry are provided. Furthermore, our method enables the experimental determination of descriptors for the activity and selectivity of catalysts. This empirical validation underlines the robustness and applicability of our approach in the characterization of catalysts and highlights the benefits of the technique.

METHODS

The catalysts were synthesized and characterized according to rigorous protocols in the framework of a data-centric approach to heterogeneous catalysis.[37] Catalyst synthesis, characterization and catalytic properties in alkane oxidation have been reported elsewhere.[36,37] Accordingly, the materials investigated here are polycrystalline, phase-pure compounds.

Adsorption Microcalorimetry. Adsorption energies of alkanes and alkenes were determined at 313 K using BT2.15 and MS70 Tian-Calvet type Calorimeters (SETARAM). The calorimeters were equipped with a custom-designed high vacuum and gas dosing apparatus (volumetric-barometric system)[42] and an in-house constructed high vacuum all-metal cell with batch geometry.[43] This configuration allowed hydrocarbon dosages as small as 0.02 μmol. A pressure transducer (MKS Baratron type 121) was used to detect pressure variations of 0.001 mbar. The calorimetric sensor was calibrated using a contact-free method based on the Joule effect. A dedicated vessel with a built-in electrical heater (Ohmic resistance 1 kΩ) was used to simulate the experimental vessel containing the sample, and calibration was carried out using a series of precise heat inputs. The catalysts were analyzed as 100−200 μm sieve fraction using 2.04, 2.6, 0.508, 1.914, and 1.6 g of $MnWO_4$, V_2O_5, $MoVO_x$, VPP, and $SmMnO_3$, respectively.

First, the catalysts were pretreated in the calorimeter cell under ultrahigh vacuum at 423 K for 2 h. Subsequently, the cell was cooled down to 313 K in a vacuum and transferred into the calorimeter. Hydrocarbons were stepwise introduced into the evacuated cell ($p < 3 \times 10^{-8}$ mbar), and the pressure evolution to determine the amount of the adsorbed molecule as well as the heat signal were recorded for each dosing step. Gases (Air Liquide) of 99.5−99.9% purity were adsorbed [C_2H_6 (2.5), C_2H_4 (2.5), C_3H_8 (3.5), C_3H_6 (2.5), n-C_4H_{10} (2.5), 1-C_4H_8 (2.5)].

The first adsorption experiment was finished when the heat of adsorption was dropped to about 25 kJ·mol^{-1}, and the corresponding adsorption isotherm exhibited a plateau. Then the cell was evacuated ($p_{final} \sim 10^{-8}$ mbar) at 313 K for 2 h, and a readsorption was carried out according to the procedure described above. The difference between the two adsorption isotherms determines the amount of irreversibly adsorbed species.

Calorimetry Data Evaluation. The raw data of an adsorption experiment are exemplarily shown for propene adsorption on $MnWO_4$ in the Supporting Information, Figure S1. The quantitative values derived from microcalorimetry are defined in Scheme 1.

Both the integral heat evolved Q_i and the equilibrium pressure p_i of the adsorbates were measured for dosages in small increments and plotted as a function of time for each dose added (Figure S1a). The calorimetry data were processed with the tools of the Origin software. Figure S1b shows the differential heat, q^{diff} (molar heat of each dose of adsorbate), as a function of the adsorbed amount n_{ads} (eq 1).

$$q^{diff} = f(n_{ads}) \quad (1)$$

https://doi.org/10.1021/acscatal.4c01308
ACS Catal. 2024, 14, 12581−12591

Scheme 1. Definition of the Quantitative Values Derived from the Microcalorimetric Experiments

q_0 heat of adsorption q^{diff} at $\theta \equiv 0$ [kJ · mol^{-1}] (3)

$q_{max} \equiv q^{diff}$ at maximum $\frac{dn_{ads}}{dq^{diff}}$ [kJ · mol^{-1}] (4)

$q_{total} = \frac{\sum_{i=1}^{N} Q_i}{\sum_{i=1}^{N} n_i}$ [kJ · mol^{-1}] (5)

q^{diff} molar heat of each dose of adsorbate (differential heat)

Θ coverage $\Theta = N/N_{total}$

N number of adsorbed molecules at each step

N_{total} number of adsorption sites in a monolayer

n_{ads} total amount of adsorbed molecules defined as sum of molecules adsorbed with q^{diff} >25 kJ·mol^{-1}

Q_i integral heat of a single adsorption event i in kJ

n_i amount adsorbed molecules at each step in mol

For an easier comparison of the heat profiles of hydrocarbons on various oxide surfaces, the results were presented as adsorption energy distribution spectra (eq 2, Figure S1c).[10−12]

$$f(q^{\mathrm{diff}}) = \frac{\mathrm{d}n_{\mathrm{ads}}}{\mathrm{d}q^{\mathrm{diff}}} \tag{2}$$

Differential heats of adsorption usually decrease with increasing surface coverage. To reduce the error of differentiation, the data were sorted so that q^{diff} decreases evenly. The fitted differential heat profile was then replotted as $n_{\mathrm{ads}} = f(q^{\mathrm{diff}})$ (red dashed line in Figure S1b), and the function was differentiated (Figure S1c). In Figure S1c, the y axis corresponds to the fractional occurrence (in %) of adsorption sites with a given heat of adsorption from the total number of adsorption sites, which is defined as $\mathrm{d}n_{\mathrm{ads}}/\mathrm{d}q^{\mathrm{diff}} \cdot n_{\mathrm{ads}}{}^{-1}$, and which is set to 100%. The area under this curve represents the number of probe molecules that were adsorbed with a given evolved heat.[44]

Various specific heats are defined (Scheme 1). The heat measured when the molecule adsorbs on an empty surface (θ = 0) is called q_0, the heat for the most abundant adsorption centers as q_{max} and q_{total} corresponds to the integral heat normalized to the total number of adsorbed molecules in a monolayer (θ = 1).

Propane Oxidation. The catalysis data were taken from a previous publication.[37] Since TOFs were calculated from these data and the adsorption data obtained in the present work, the formulas used to calculate the conversion of propane $X_{C_3H_8}$ (eq 6), the selectivity S_i to product i (eq 7), and the consumption and formation rates (eqs 8−10) of propane ($r_{C_3H_8}$) and the various products ($r_{CO_2,C_3H_6,C_xH_yO_z}$), respectively, are given below

$$X_{C_3H_8} = \frac{\sum_{i=1}^{n} N_i c_i}{\sum_{i=1}^{n} N_i c_i + 3 \times c_{C_3H_8}} \times 100 \tag{6}$$

$$S_i = \frac{N_i c_i}{\sum_{i=1}^{n} N_i c_i} \times 100 \tag{7}$$

where N_i is the number of carbon atoms in the product i, c_i is the concentration of the product i in the gas leaving the reactor, and $c_{C_3H_8}$ is the concentration of propane in the gas leaving the reactor.

The rates of C_3H_8 consumption, and C_3H_6, $C_xH_yO_z$ and CO_2 formation have been calculated using the following equations

$$r_{C_3H_8} = \frac{X_{C_3H_8}}{\left(\frac{W}{F}\right)} \tag{8}$$

$$r_i = r_{C_3H_8} \times \frac{N_i c_i}{\sum_{i=1}^{n} N_i c_i} \tag{9}$$

where i is C_3H_6, $C_xH_yO_z$ or CO_2, W is the mass of the catalyst in g, and F is the total flow rate in L·h^{-1}.

The turnover frequency of propane consumption was determined using the integral propane consumption rate at 548 K, which is the lowest reaction temperature at which all catalysts were active

$$\mathrm{TOF}_{C_3H_8} = \frac{r_{C_3H_8}}{n_{\mathrm{ads}(C_3H_8)}} \tag{10}$$

where $n_{\mathrm{ads}(C_3H_8)}$ is the total amount of adsorbed propane in a monolayer (adsorption capacity) as measured by adsorption calorimetry at 313 K (Table 1).

The turnover frequency for oxygenate formation at 548 K was calculated as follows

$$\mathrm{TOF}_{C_xH_yO_z} = \frac{r_{C_xH_yO_z}}{n_{\mathrm{ads}(C_3H_6)}} \tag{11}$$

where $n_{\mathrm{ads}(C_3H_6)}$ is the surface monolayer adsorption capacity of propene as measured by adsorption calorimetry at 313 K (Table 1), and $r_{C_xH_yO_z}$ is the oxygenate formation rate at 548 K. Oxygenates involve acetic acid, acrylic acid, acetone, propanal, and propionic acid. Further experimental details can be found in the Supporting Information.

Table 1. Specific Surface Area S,[37] Adsorption Capacity n_{ads}, Heats of Adsorption q of Propane and Propene at 313 K

ID[a]	formula	S, m^2·g^{-1}	n_{ads}, μmol·g^{-1}		q_0, kJ·mol^{-1}		q_{max}, kJ·mol^{-1}		q_{total}, kJ·mol^{-1}	
			C_3H_8	C_3H_6	C_3H_8	C_3H_6	C_3H_8	C_3H_6	C_3H_8	C_3H_6
32024	$MnWO_4$	35	6.4	50	35	69	35	42	32	49
31034	V_2O_5	5	0.16	3.4	82	84	30	46	30	56
31012	$MoVO_x$	61	4.4	58.2	35	100	30	95	31	67
31650	VPP	20	0.25	24.2	97	141	30	140	30	105
30869	$SmMnO_3$	7.5	4.5	2.6	64	338	45	320	46	138

[a]Unique sample ID of the synthesized batch to distinguish reproductions in catalyst synthesis.

https://doi.org/10.1021/acscatal.4c01308
ACS Catal. 2024, 14, 12581−12591

RESULTS

Determination of Adsorption Energy Distributions. The adsorption of alkanes and alkenes was performed at 313 K. Alkane oxidations over the materials investigated involve complex reaction networks in which a multitude of secondary and parallel transformations can occur.[45] The alkene is the first intermediate in a consecutive reaction that leads to oxygenated products, such as acrolein or acrylic acid, and finally to undesired CO_2, as schematically shown in eq 12.

$$C_3H_8 + O_2 \rightarrow C_3H_6 \rightarrow \text{oxygenates} \rightarrow CO_2 \quad (12)$$

Figure 1a shows the differential heat of adsorption (q^{diff}, further also denoted as q) as a function of coverage measured

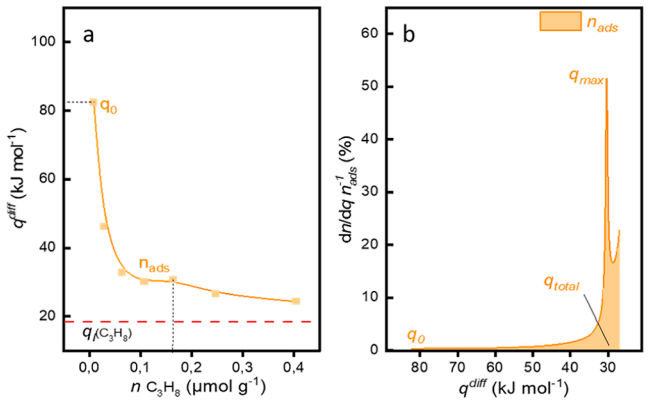

Figure 1. Propane adsorption on V_2O_5 measured by microcalorimetry at 313 K; (a) differential heat profile, i.e., the heat of adsorption measured as a function of the amount of adsorbed molecules and (b) adsorption energy distribution spectrum, i.e., the number of adsorption sites as a function of the heat of adsorption $(dn_{ads}/dq^{diff})\cdot n_{ads}^{-1} = f(q^{diff})$, (see eq 2).

on V_2O_5 during stepwise propane dosing (eq 1). The heat decreases with each step and eventually approaches the heat of condensation of propane (q_l = 16 kJ·mol^{-1}). The monolayer is completed when the heat of adsorption approaches a plateau, indicating that all adsorption sites on the surface of the catalyst are occupied. The plateau, i.e., the total amount of adsorbed molecules n_{ads} in the monolayer (also called adsorption capacity, Table 1) is reached at a slightly higher heat of 20−30 kJ·mol^{-1} (marked with a dotted line in Figure 1a for V_2O_5) compared to the heat of condensation of propane most likely due to significant adsorbate−adsorbate interactions in the monolayer.[44] This is the energy range of physisorption, which is also indicative for multilayer formation.[44]

Differentiation of the function shown in Figure 1a gives the energy distribution spectrum of propane adsorption on V_2O_5 (Figure 1b). The adsorption energy distribution spectra should not be interpreted as a snapshot of the pristine surface at a given moment but as its evolution with increasing partial pressure of the adsorbate, i.e., with increasing coverage.

Mapping the number of adsorption sites as a function of the heat of adsorption by recording energy distribution spectra allows a quick and direct comparison of the energetic profiles of different catalyst surfaces (Figures 2 and S2). From these graphs, information about the diversity of adsorption sites can be obtained at first glance. In addition, the strength of the interaction of the adsorbates at the solid−gas interface becomes apparent.[10−12,43,46,47] This method gives direct access to quantitative values, such as the heat q_0 obtained when a molecule is adsorbed on the empty surface (definition in eq 3 in Scheme 1), which generally characterizes the strongest adsorption sites if lateral adsorbate−adsorbate interactions[24,48] or possible restructuring of the surface in the course of the adsorption experiment do not lead to unusual patterns.[49] The heat q_{max} represents the heat of adsorption at the most abundant adsorption sites on the surface (definition in eq 4 in Scheme 1). Furthermore, the total heat q_{total} is determined by summing up all the evolved heat divided by the total number of adsorbed probe molecules n_{ads}, which gives an average information on the overall strength of the adsorbate interaction with the surface (eq 5 in Scheme 1). In the following, the differences between the catalysts for both propane and propene adsorption are discussed (Figure 2). The heat of adsorption as a function of coverage and readsorption experiments for all hydrocarbons investigated in the present study are shown in Figure S2.

Adsorption of Propane. Propane is weakly and reversibly adsorbed (q_{max} < 50 kJ·mol^{-1}) on all surfaces (Figures 2a and S2a,b), with the heat of adsorption on the most abundant energetic sites q_{max} showing the following trend: V_2O_5 = $MoVO_x$ = VPP < $MnWO_4$ < $SmMnO_3$ (for numerical values see Table 1). Compared to the adsorption of propane on the 001 single crystal surface of V_2O_5 (37 ± 5 kJ·mol^{-1}), the heat for the most abundant adsorption centers on the polycrystalline V_2O_5 studied here is slightly lower at 30 kJ·mol^{-1}.

Even though most of the adsorption sites on $SmMnO_3$ and VPP interact only weakly with propane, there are a few sites on these surfaces that reveal strong interaction, resulting in higher values of q_0 of 64 kJ·mol^{-1} for $SmMnO_3$ and especially of 97 kJ·mol^{-1} for VPP (Figure 2a, Table 1).

In general, the span in the energy of adsorption and the width of the individual peaks indicate the degree of (in)homogeneity of the surface and, thus, the diversity or uniformity of the adsorption sites.

The width of the adsorption range for VPP and V_2O_5 points to a particular energetic diversity of these surfaces. This is strikingly different from the adsorption of hydrocarbons on zeolites, where energetically very uniform adsorption centers are present.[49,50] Likewise, on the chemically even more complex oxidation catalyst $MoVTeNbO_x$, an adsorption isotherm was measured in which the boundary conditions of a Langmuir isotherm with respect to uniformity of the adsorption sites and absence of adsorbate−adsorbent interactions are clearly better fulfilled than in the case of the vanadates investigated here.[46] For the materials studied in the present work, it should be noted that adsorbate−adsorbate interactions in pores and confinement effects do not significantly affect the present results because the samples have a comparatively small specific surface area and no microporosity (Table 1).

Adsorption of Propene. Propene, as the first stable and desorbable reaction product in the consecutive oxidation of propane reveals much stronger interaction and a broader adsorption energy spectrum than propane (Figures 2b and S2c,d). The energy of the most abundant propene adsorption sites q_{max} shows the following trend: $MnWO_4$ ≈ V_2O_5 < $MoVO_x$ < VPP < $SmMnO_3$ (Table 1). Propene covers a considerably wider range of strong chemisorption (100−150 kJ·mol^{-1}) and reactive adsorption (200−350 kJ·mol^{-1}) than propane.

All catalysts exhibit several kinds of adsorption sites with discrete energy values. The $SmMnO_3$ perovskite contains two

https://doi.org/10.1021/acscatal.4c01308
ACS Catal. 2024, 14, 12581−12591

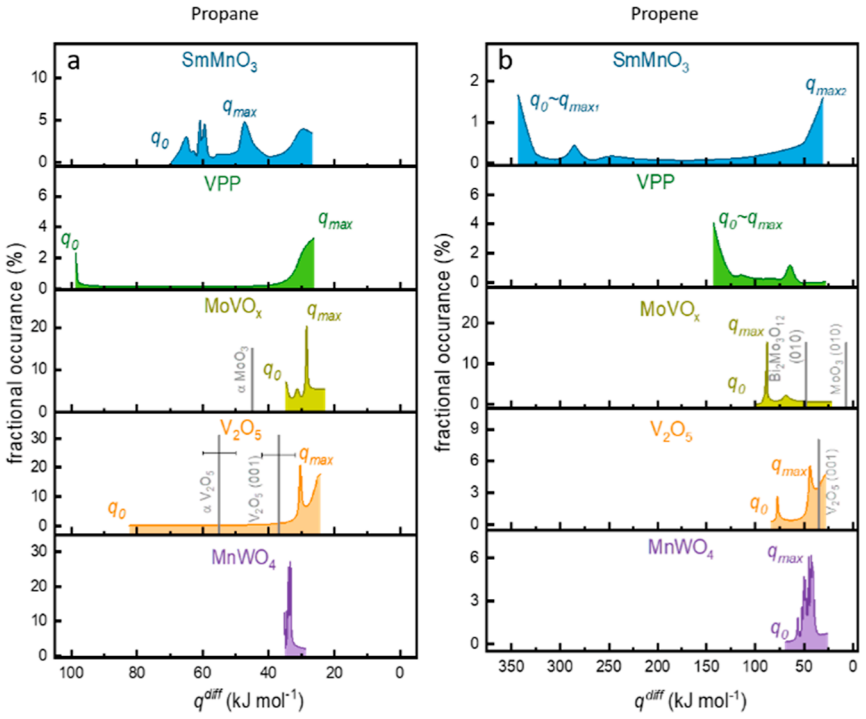

Figure 2. Adsorption energy distribution spectra, i.e. the number of adsorption sites as a function of the heat of adsorption $(dn_{ads}/dq^{diff})\cdot n_{ads}^{-1} = f(q^{diff})$, (see eq 2), of (a) propane and (b) propene at 313 K determined by measuring the heat of adsorption by microcalorimetry as a function of coverage (Figure S1b), which was determined based on a simultaneously performed volumetric measurement of the adsorbed amount (determination of the adsorption isotherm $n_{ads} = f(p)$); Bars denote the heat of adsorption taken from the literature and determined experimentally on single-crystal references and polycrystalline reference compounds for propane on V_2O_5 (001),[51] α-V_2O_5, and α-MoO_3,[47] and values calculated by DFT for propene adsorption on V_2O_5 (001),[52,53] oxygen terminated planes of $Bi_2Mo_3O_{12}$ (010),[54] MoO_3 (010),[54] and clusters of Mo_3O_9;[55] All spectra are shown to the energy of 25 kJ·mol^{-1}, which corresponds to the beginning of multilayer formation; The heats of adsorption of the molecules on an empty surface q_0 and on the most abundant adsorption sites q_{max} (Scheme 1) are indicated; The numerical values are provided in Table 1; For the differential heat profiles please see Figure S2a,c.

groups of most abundant sites, where high-energy sites with $q_{max1} \sim 350$ kJ·mol^{-1} and physisorption sites with $q_{max2} \sim 30$ kJ·mol^{-1} are evenly distributed. The energy distribution on V_2O_5 matches the V_2O_5 (001) single crystal reference well but features a considerable additional peak near $q_0 = 76$ kJ·mol^{-1}. This heat is in accordance with the reaction energy of propene activation.[52] Subsequent readsorption after evacuation at the adsorption temperature of 313 K shows that the strong sites are no longer available for propene on all catalysts except $MoWO_4$, where blocking of the sites occurs only to a limited extent (Figure S2c,d). Here, weak adsorption sites associated with reversible interaction with $q < 65$ kJ·mol^{-1} are accessible for readsorption.

Diffuse reflectance infrared Fourier transform spectroscopy (DRIFTS) confirms reactive adsorption and blockage of adsorption sites (Table S1 and Figure S3a–d). $MoVO_x$, VPP, and $SmMnO_3$ with high energy centers ($q_{max} > 80$ kJ·mol^{-1}) transform adsorbed propene to oxygenates already at room temperature by a redox reaction with the catalyst, as evidenced by the appearance of bands due to C–O and C═O stretching vibrations in the region between 1750 and 1400 cm^{-1} upon propene adsorption at 313 K. The intense bands between 1650 and 1600 cm^{-1} due to C═C stretching modes and 1450–1320 cm^{-1} due to C–H deformation modes confirm, in addition, the irreversible binding of the propene molecules even after evacuation to 10^{-6} mbar on all catalysts (Figure S3e). Peaks at 1595 and 1571 cm^{-1} for the perovskite (Figure S3a) indicate the evolution of conjugated C–O/C═O groups, which agrees with the exceptionally high energies of 200–350 kJ·mol^{-1} in the reactive adsorption of propene on $SmMnO_3$ (Figure 2b). The peaks at the higher wavenumbers 1695 and 1672 cm^{-1} are associated with C═O stretching modes of carbonyl groups.[56,57] In contrast, $MnWO_4$ with narrowly distributed chemisorption sites ($q_{max} = 42$ kJ·mol^{-1}) interacts gently with propene in line with the bands at 1608 and 1635 cm^{-1} ascribed to the C═C stretching vibrations of propene weakly π-bonded to two different adsorption sites (Figure S3d). However, the shoulder at 1661 cm^{-1} also indicates carbonyl groups forming on this catalyst. A combination of flow calorimetry and mass spectrometry confirms that no gaseous products are released at the adsorption temperature of 313 K (Figure S4). Therefore, we also exclude the desorption of oxygenates, CO_2 or H_2O in the microcalorimetric experiments. This means we rule out a falsification of the measured equilibrium pressures by products that desorb. Thus, the heat released during the adsorption of propene, results from a superposition of heat due to reversible adsorption and reaction heat, the latter being liberated due to the formation of strongly adsorbed surface species.

Adsorption Capacities of Propane and Propene. Regardless of structure and composition, all catalysts provide a low capacity of ~0.1–6 μmol·g^{-1} for the adsorption of propane at 313 K that does not correlate with the specific surface area determined by nitrogen adsorption at 77 K (Figure S5a, Table 1). The density of propane adsorption sites is comparable on all catalysts and scatters around 0.1 nm^{-2} (Figure S5b). In contrast, the amount of C_3H_6 increases significantly with the specific surface area of the materials

https://doi.org/10.1021/acscatal.4c01308
ACS Catal. 2024, 14, 12581–12591

(Figure S5a, Table 1), which is consistent with more specific adsorption of the alkene. Furthermore, a higher surface density of the adsorbed species is observed. For example, adsorbed propene shows an increased density of adsorption sites of approximately 0.8 molecules nm^{-2} on VPP and $MnWO_4$ (Figure S5b). The differences are due to the different chemical interactions of propane and propene, which can occur on the one hand via the hydrogen atoms of the adsorbed molecule to surface oxygen atoms or via a carbon atom or the C=C bond in case of the olefin to Lewis acid centers.

Influence of the Hydrocarbon Chain Length. The heat of adsorption at the most abundant adsorption sites on the surface q_{max} does not correlate with the carbon number in the adsorption experiments of C2−C4 alkanes (Figure S6a), suggesting weak and unspecific adsorption of alkanes on the investigated materials, and differing from what has been reported on zeolites.[49]

There is also no trend with the energy of the weakest methylene C−H bond, as the difference in energies for C2−C4 alkanes is small, not exceeding 10 $kJ{\cdot}mol^{-1}$ (Figure S6b). For the alkene, however, the interaction between H atoms and oxygen atoms is relevant because q_{max} scales linearly with the carbon chain length for the adsorption of the homologous C2−C4 alkenes (Figure S6c). In addition, the strength of the weakest C−H bond in the olefin shows a negative correlation with q_{max} (Figure S6d). This means that the less strong the weakest C−H bond in the olefin (444 $kJ{\cdot}mol^{-1}$ for ethene, 361 $kJ{\cdot}mol^{-1}$ for propene, and 345 $kJ{\cdot}mol^{-1}$ for 1-butene),[58,59] the stronger the interaction with the catalyst. In other words, the interaction between ethene and the catalysts is the weakest, followed by propene and 1-butene. However, the difference in the heat of adsorption of the homologous alkenes varies for each surface. For example, there is virtually no difference between ethene and 1-butene for $MnWO_4$, a difference of about 100 $kJ{\cdot}mol^{-1}$ for $MoVO_x$ and VPP, and a significant difference of about 450 $kJ{\cdot}mol^{-1}$ for $SmMnO_3$ (Figure S6d). This could be due to variations in the Lewis acidity of the surfaces studied and to the change in proton affinity of the alkenes with altering chain length.[59] The positive induction effect, growing with an increasing chain length of the alkyl group at the C=C double bond, should cause an increase in the basicity of ethene via propene to 1-butene in the gas phase. The strong dependence of the heat of adsorption on the chain length measured on $SmMnO_3$ (Figure S6d) suggests that the interaction via the C=C double bond with Lewis acidic centers dominates the adsorption of alkenes on the perovskite. The differences in the interaction of the catalysts studied here with reactants and intermediates can explain the differences in the reactivity in alkane oxidations, in particular the differences in selectivity. In the following, we analyze and discuss this based on the example of propane oxidation.

From Adsorption to Reaction. The adsorption energy distribution spectra show that all catalysts exhibit a more or less heterogeneous distribution of adsorption sites (Figure 2). Thus, it can be assumed that not every site is equally responsible for the processes of bond rearrangement in alkane oxidation. Likely, all of them contribute to the overall performance in a complex manner owing to a combination of geometric, electronic and confinement parameters.[60]

Since propane adsorption on all catalysts is similar and unspecific, the heat of adsorption of the most abundant sites determines the total heat value (Figure S7a). For propene adsorption, however, there is a linear relationship between q_{total} and q_{max}. The slope of 0.35 means that q_{max} contributes significantly to the total heat of propene adsorption for all catalysts studied in the present investigation. Frequently, q_0 is used in modeling and interpreting catalysis data, while q_{max} is hardly ever considered. Indeed, the initial heat of propane adsorption on the different catalysts varies (black open squares in Figure S7b and Table 1), while q_{max} remains relatively constant. In contrast, a linear correlation with a slope approaching 1 is obtained when plotting q_{max} as a function of q_0 in case of propene adsorption (red symbols in Figure S7b). This means that in propene adsorption, the energy of the frequently occurring sites mainly corresponds or is close to the initial heat of adsorption.

Comparing the adsorption of propane and propene in a single contour plot for multiple catalysts is informative, as these two molecules constitute a common reaction network.[47] Propene is the first intermediate product in propane oxidation (eq 12). Correlation diagrams of the adsorption energy distribution of propane and propene (Figure 3) are particularly instructive as an orientation map through the whole array of bonding possibilities on multifaceted surfaces. The intensity in the contour plot reflects the number of adsorption sites. A relatively narrow energetic distribution of propane adsorption sites is found for $MnWO_4$ and $MoVO_x$, while the distribution

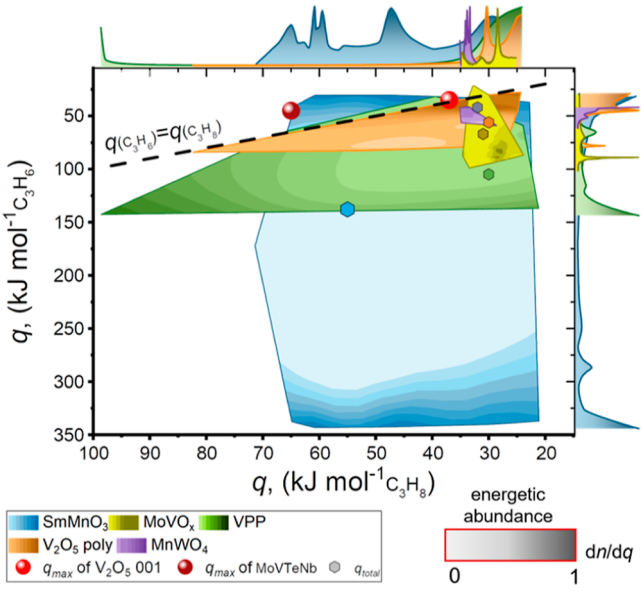

Figure 3. Adsorption-strength covariance diagram of propane and propene illustrating the energetic abundance (fractional occurrence) as a correlation parameter to analyze the relationship between propene and propane adsorption energies in the adsorption spectra; This 2-D covariance diagram shows the various bonding possibilities for the two molecules, which occur in the common reaction network of propane oxidation; The color indicates the catalyst, the shading the abundance of molecules adsorbed with this energy; This diagram serves as a model, providing an energetic snapshot of the pristine surface; Filled spheres correspond to the position of q_{max} for literature data of propane and propene adsorption on the MoVTeNb catalyst[47] and on the V_2O_5 (001) single crystal surface;[51−53] The hexagons are the position of q_{total} of propane and propene for a given catalyst; The dashed line is a hypothetical line where the heat of adsorption on the most abundant centers for propane and propene is equal ($q_{max}(C_3H_8)$ = $q_{max}(C_3H_6)$); The diagram acts as a model and conveys the adsorption energy of the specific molecule aside from the spatiotemporal aspect.

https://doi.org/10.1021/acscatal.4c01308
ACS Catal. 2024, 14, 12581−12591

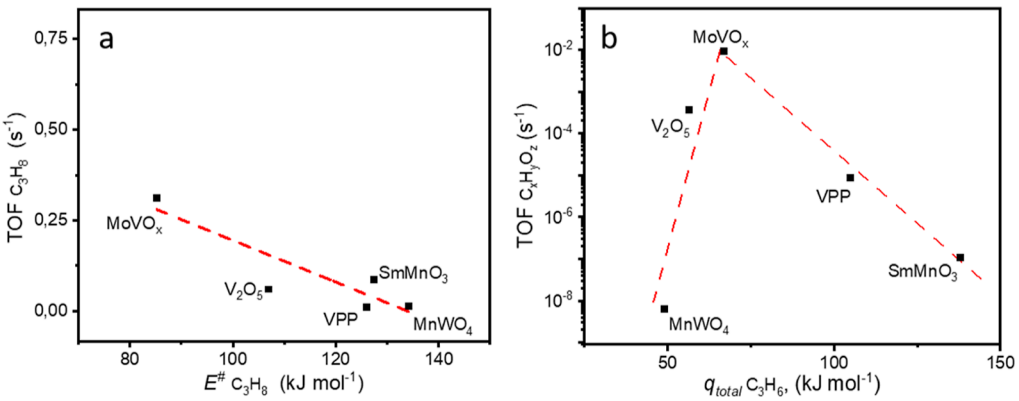

Figure 4. (a) Turnover frequency based on the propane consumption rate measured in steady-state at 548 K [$r(C_3H_8)/n_{ads}(C_3H_8)$], where $n_{ads}(C_3H_8)$ is the total amount of adsorbed propane in a monolayer (adsorption capacity), as a function of the activation barrier for propane oxidation calculated as $q_{total} + E_a^{app}$, where q_{total} is the total adsorbed amount weighted heat of propane and E_a^{app} is the apparent activation energy of propane consumption (Figure S8b); (b) turnover frequency based on the oxygenate formation rate [$r(C_xH_yO_z)/n_{ads}(C_3H_6)$] as a function of q_{total} of propene; oxygenates involve acetic acid, acrylic acid, acetone, propanal, and propionic acid. The TOF values are estimated under the assumption that the adsorption at 313 K is also representative for the surface at 548 K and that propane is only converted at C_3H_8-specific adsorption sites and the oxgenates are only formed at C_3H_6-specific adsorption sites.

at the perovskite is broader. For V_2O_5 and VPP, on the other hand, the distribution of propane adsorption heats is very broad. The perovskite, conversely, shows a vast range of energies for the propene adsorption sites.

Although it is immediately apparent from a simple inspection of the correlation plot which catalysts adsorb propene more weakly than propane (data above the dashed line in Figure 3), and should therefore be comparatively selective for propene formation, general conclusions about selectivity to the various products that can occur in propane oxidation are not so straightforward. However, the measured data, in combination with the catalytic data, can form the basis for evaluation using machine learning methods to predict selective catalysts for complex reactions, which, however, goes beyond the scope of the present experimental work.

The catalytic performance of the five catalysts has been measured in an extensive campaign according to standard operating procedures and published elsewhere for propane oxidation over the vanadium-containing catalysts,[36] and the oxidation of C2−C4 alkanes over all catalysts.[37] Based on the adsorption data determined in the present work, it is now possible to calculate TOF (Figure 4). The catalysis data used for the calculation are recompiled in Figure S8 for discussion in this paper. The activity decreases in the order $MoVO_x$ > $SmMnO_3$ > $MnWO_4$ > V_2O_5 ≈ VPP (Figure S8a). This sequence is not reflected in the apparent activation energies, which increase as follows: $MoVO_x$ < V_2O_5 < VPP < $SmMnO_3$ > ≈$MnWO_4$ (Figure S8b). This trend confirms earlier indications that propane oxidation on manganese-containing catalysts proceeds according to a different mechanism than on the vanadium-containing catalysts, especially as far as the regeneration of the active sites is concerned, which could become rate-relevant here.[30]

For all catalysts, the TOF decreases with increasing activation barrier (Figure 4a). The TOF was calculated based on the integral propane consumption rate normalized to the adsorption capacity of propane n_{ads} determined by microcalorimetry (eq 10, Table 1). According to eq 13, the activation barrier is the sum of the apparent activation energy of propane consumption (Figure S8b) and the heat of propane adsorption measured by microcalorimetry (Table 1).[61]

$$E^{\#} = E_a^{app} + q \tag{13}$$

The two kinetic parameters integral propane consumption rate and apparent activation energy were measured in a fixed bed reactor and thus represent the average catalytic activity of the surface over the entire catalyst bed. Interestingly, the correlation between TOF and $E^{\#}$ is only found when the total heat (q_{total}), but not q_0 or q_{max}, and the total number of molecules adsorbed (n_{ads}) are used to calculate the TOF (Figure 4a). This is impressive evidence that all propane adsorption sites contribute to the propane consumption rate on the investigated mixed oxides, underlining that the overall activity (typically measured in the catalytic reactor) is a "weighted distribution of activities among different active sites", i.e., an average of the activities of each available site for each reaction step, weighted by the energetic importance of that step and the concentration of the corresponding site on the investigated material.[60]

At low conversions, all catalysts show some selectivity to propene (Figure S8c) that can be further oxidized to oxygenates and carbon oxides. According to Sabatier's principle, maximum formation rates can be expected at medium adsorption strength for reactants or products depending on the nature of the transition state.[62]

In the present work, the maximum turnover frequency of the formation of oxygenates is found at $MoVO_x$, which has medium heats of adsorption for the intermediate propene (Figure 4b). Again, the total heat of propene adsorption on the surface (q_{total}) is the basis for the correlation. The adsorption sites on the surface of VPP are highly inhomogeneous and distributed over a wide range of adsorption energies for propane and propene (Figures 2 and 3). This variety of adsorption sites leads to the most diverse product distribution $CO_2/C_3H_6/CO$/oxygenate = 19/14/32/33 among the five catalysts (Figure S9). Given the diversity of mechanisms discussed in propene oxidation, such as here in DFT studies of Mo-,[63] and V-based systems,[52,64] the simple relationship shown in Figure 4 b is surprising. The nature of the transition state depends on the composition and defect structure of the catalyst as well as the reaction path or selective oxidation product formed. Therefore, no mechanistic conclusion should

https://doi.org/10.1021/acscatal.4c01308
ACS Catal. 2024, 14, 12581−12591

be drawn from the present experimental observation, as phenomena can overlap. Nevertheless, the integral heat of propene adsorption seems to be a global indicator for the selectivity of the structurally different and representative catalyst materials investigated in the present study.

In summary, the heat q_{total} appears to be an essential parameter for predicting the performance of a selective oxidation catalyst, even if q_{total} is measured under conditions (low equilibrium pressures, 313 K) that are far from the conditions of catalysis. Interestingly, this descriptor could be identified, although it is known that the surface of the materials investigated here is generally subject to restructuring under working conditions.[33−35,37,65−67] However, the trends measured on the fresh catalysts appear to be maintained. The stability of the bulk phase under reaction conditions is undoubtedly an essential requirement.

Limitations and Further Development. The presented approach is limited in that microcalorimetry cannot be applied operando. To provide a better understanding, a potential solution is to compare freshly synthesized catalyst precursors with catalysts that have been activated under reaction conditions or deactivated catalysts.

While flow calorimetry has the potential for operando studies,[68] it presents challenges in differentiating the heats of reaction from those caused by phase transformations of the catalyst under reaction conditions and heats of adsorption. Conversely, microcalorimetry can discern between adsorption processes and chemical reactions by analyzing the heat profiles released during dosing (Figure S1a).

Particularly at the reaction temperature, but in general, there is a challenge with regard to the detection limit if only a few adsorption sites are available on the surface of the catalyst due to low specific surface area and/or low site density or if the adsorption constants are small. The detection limit depends on the sensitivity of the employed technique. The maximum calorimetric sensitivity for the equipment used in this work is 40−50 μV/mW for microcalorimetry and 7 μV/mW for flow calorimetry. In addition to the superior sensitivity of the microcalorimeter, the equipment utilizes larger cells, enabling the handling of sample loadings that are 10 times greater than that achievable with a flow calorimetry reactor. In practice, the microcalorimetric setup we use can detect surface concentrations down to 0.02 μ mol·m^{-2} for energies of 40−60 kJ mol^{-1}.[43]

Essentially, all catalyst materials can be investigated using the present approach. The materials do not necessarily have to be homogeneous. However, homogeneity in terms of volume and surface properties, such as phase purity and narrow particle size distributions, facilitates the interpretation of the data.

Another limitation of microcalorimetry is the comparatively long time required for recording complete adsorption isotherms. The heat q_{total} can also be measured much faster using flow calorimetry in a fixed bed reactor, allowing for the accelerated screening of larger material libraries.

Despite these limitations, the acquisition of energy distribution spectra by microcalorimetry in combination with operando or in situ vibrational spectroscopy of adsorbed reactants, intermediates and products can support the theory in the development of realistic models for surface structures of complex high-performance catalysts by matching adsorption enthalpies of a variety of hypothetical models and adsorption complexes with experimental values.

GENERAL DISCUSSION

The way the kinetics of a catalytic reaction is generally described is based on the principles of Langmuir adsorption and the kinetic formalism of Hinshelwood, assuming ideal surfaces with equivalent adsorption sites and adsorbates that are randomly distributed and do not interact. The current investigation of complex metal oxides in reactions subject to complicated reaction networks shows that the actual situation is far more intricate and requires more than the distinction between active and resting sites. This is a frequently argued assumption, but the strength of the adsorption of reactants on the surface of real high-performance catalysts has never been experimentally quantified for such a set of diverse materials.

In the present work, we did this by measuring the energy distribution spectra of adsorbed reactants and intermediates in propane oxidation. Since a catalyst can have multiple surface centers and adsorption is coverage-dependent, many simultaneous reaction pathways are possible. Each site is differently active and contributes to the overall reaction rate as a nonlinear superposition of multiple rates. A parallel can be drawn here to the empirical structure−sensitivity relationship for CO_2 reduction over a nickel catalyst, where each of the Ni facets contributes differently to the target reaction for a given particle size.[69,70] Moreover, depending on adsorbate coverage, the dynamic adlayer experiences lateral interactions that already result in a distribution of adsorption energies, as shown for CO adsorption on Pt and Co single facets.[24,48] To account for this complexity, adsorption and catalysis data are essential to support studies using computational chemistry. Thus, machine learning methods may be able to predict which interaction (heat of adsorption) is required for the formation of a certain product in complex reactions. This could also be used to derive material properties that need to be adjusted during the synthesis and formation of a selective catalyst.[37]

However, microcalorimetric measurements are not routine investigations and are comparatively time-consuming (1 day to 2 weeks per sample). Therefore, data science techniques that can cope with small data sets are required for their evaluation. But, if q_{total} is relevant, as in the present reaction, flow calorimetry can provide integral heats much faster and, if necessary, also in parallel. Furthermore, if measured according to well-defined protocols and documented in consistent formats, microcalorimetric data can also be collected in publicly accessible repositories that can provide much more extensive data sets over time, which can then be analyzed in many different ways. This can accelerate discoveries in all interface-based sciences that deal with functional materials.

Finally, it should be emphasized that with so many different unspecific adsorption centers on complex oxide catalysts, i.e., diversified binding possibilities, there cannot be only one descriptor, but an interplay of different adsorption sites is always responsible for the activity and selectivity measured in a fixed-bed reactor in complex reactions such as the selective oxidation of propane. Consequently, kinetic models must replace the "active sites", generally symbolized by "*", with active site distributions to realistically describe complex reactions on multifaceted interfaces. These distributions of active sites can be determined using the method presented in this paper. Reaction rates would then become probability functions controlled by the shape of the adsorption energy distribution spectra.

https://doi.org/10.1021/acscatal.4c01308
ACS Catal. 2024, 14, 12581−12591

CONCLUSIONS

Adsorption microcalorimetry can be used as a complementary technique to e.g. operando spectroscopy and in situ electron microscopy[71] to analyze and map the energetic distribution of adsorption sites on catalyst surfaces of complex composition when investigating the adsorption of reactants at temperatures below the reaction temperature.

Despite the phase purity of the bulk catalysts studied here, it is clear that even in binary oxides the surface generally shows a distribution of adsorption sites, also due to differences in the surface structure compared to the bulk. The present work therefore clearly supports the thesis that the bulk structure cannot be solely responsible for the reactivity, i.e., the ideal configuration in the crystalline volume phase cannot be used as a basis for extrapolating the surface structure, but the nature of the surface centers should be verified experimentally.

Using the measured total heat q_{total} of propane adsorption and the apparent activation energy determined in a fixed-bed reactor in propane oxidation, activation barriers can be estimated experimentally, the trend of which corresponds to the trend of the activity of the investigated catalysts.

Furthermore, it can be shown experimentally that the highest turnover frequency for the formation of valuable oxygenates in propane oxidation is obtained with medium strong binding of the intermediate propene to the surface of the catalyst. Thus, the total heat q_{total} of propene adsorption determined by microcalorimetry can be used as a descriptor for the prediction of selective oxidation catalysts.

Our method provides experimental reference values for the validation of computational approaches. The experimental adsorption energy distribution spectra can be aligned with computational techniques such as machine learning and linear scaling DFT methods developed to increase the speed of obtaining realistic atomistic models for heterogeneous catalysis,[18] as well as DFT functionals that enable the calculation of increasingly accurate total energies to account for surface irregularities, stacking faults, grain boundaries and defects in real high-performance catalysts. Rigorous experimentation,[36,37,72] and the availability of adsorption data for complex materials in publicly accessible databases can thus make an essential contribution to the faster development of new data science methods and sophisticated electron structure calculations based on first-principles for the accelerated discovery of improved functional materials.

ASSOCIATED CONTENT

Supporting Information

The Supporting Information is available free of charge at https://pubs.acs.org/doi/10.1021/acscatal.4c01308.

Description of further experimental details regarding microcalorimetry, flow calorimetry, DRIFTS and nitrogen adsorption, an assignment of the observed bands in the DRIFT spectra, an example of raw data of the microcalorimetric measurements, all evaluated data of propane, propene, *n*-butane, 1-butene, ethane and ethene adsorption, DRIFTS spectra of adsorbed propene, raw data of flow calorimetry, further data analysis of the microcalorimetric data, results of the catalytic test in propane oxidation, further references (PDF)

AUTHOR INFORMATION

Corresponding Author

Annette Trunschke − *Department of Inorganic Chemistry, Fritz-Haber-Institut der Max-Planck-Gesellschaft, D-14195 Berlin, Germany*; orcid.org/0000-0003-2869-0181; Email: trunschke@fhi-berlin.mpg.de

Authors

Andrey V. Tarasov − *Department of Inorganic Chemistry, Fritz-Haber-Institut der Max-Planck-Gesellschaft, D-14195 Berlin, Germany*

Sabine Wrabetz − *Department of Inorganic Chemistry, Fritz-Haber-Institut der Max-Planck-Gesellschaft, D-14195 Berlin, Germany*

Jutta Kröhnert − *Department of Inorganic Chemistry, Fritz-Haber-Institut der Max-Planck-Gesellschaft, D-14195 Berlin, Germany*

Frank Rosowski − *BasCat—UniCat BASF JointLab, D-10623 Berlin, Germany; BASF SE, Catalysis Research, D-67065 Ludwigshafen, Germany*

Robert Schlögl − *Department of Inorganic Chemistry, Fritz-Haber-Institut der Max-Planck-Gesellschaft, D-14195 Berlin, Germany*

Complete contact information is available at: https://pubs.acs.org/10.1021/acscatal.4c01308

Author Contributions

The manuscript was written through contributions of all authors. All authors have given approval to the final version of the manuscript.

Funding

This work was conducted in the framework of the BasCat collaboration between BASF SE, Technical University Berlin, Fritz-Haber-Institut (FHI) der Max-Planck-Gesellschaft, and the clusters of excellence "Unified Concepts in Catalysis"/"Unifying Systems in Catalysis" (UniCat www.unicat.tu-berlin.de/UniSysCat www.unisyscat.de). Funding by the Deutsche Forschungsgemeinschaft (DFG, German Research Foundation) under Germany's Excellence Strategy—EXC 2008-390540038—UniSysCat is acknowledged. Open access funded by Max Planck Society.

Notes

The authors declare no competing financial interest.

ACKNOWLEDGMENTS

Stephen Lohr (BASF SE), Dr. Gregor Koch, and Sven Richter (FHI) are acknowledged for the synthesis of most of the materials, and Dr. Ezgi Erden and Dr. Pierre Kube (FHI) for performing the previously published catalyst tests. We thank Maike Hashagen (FHI) for carrying out the nitrogen adsorption studies.

REFERENCES

(1) Langmuir, I. The Adsorption of Gases on Plane Surfaces of Glass, Mica and Platinum. *J. Am. Chem. Soc.* **1918**, *40* (9), 1361−1403.

(2) Motagamwala, A. H.; Dumesic, J. A. Microkinetic Modeling: A Tool for Rational Catalyst Design. *Chem. Rev.* **2021**, *121* (2), 1049−1076.

(3) Stoltze, P. Microkinetic Simulation of Catalytic Reactions. *Prog. Surf. Sci.* **2000**, *65* (3−4), 65−150.

(4) Calvet, E.; Prat, H. *Récents Progrès en Microcalorimétrie*; Dunod: Paris, 1958.

(5) Gravelle, P. C. Application of Adsorption Calorimetry to the Study of Heterogeneous Catalysis Reactions. *Thermochim. Acta* **1985**, *96* (2), 365−376.
(6) Bennici, S.; Auroux, A. Thermal Analysis and Calorimetric Methods. In *Metal Oxide Catalysis*; Jackson, S. D., Hargreaves, J. S. J., Eds.; Wiley-VCH Verlag GmbH & Co. KGaA, 2009; pp 391−441.
(7) Cardona-Martinez, N.; Dumesic, J. A., Applications of Adsorption Microcalorimetry to the Study of Heterogeneous Catalysis. In *Adv. Catal.*, D.D. Eley, H. P.; Paul, B. W., Eds. Academic Press: 1992; Vol. Vol. *38*, pp 149−244, .
(8) Wellendorff, J.; Silbaugh, T. L.; Garcia-Pintos, D.; Nørskov, J. K.; Bligaard, T.; Studt, F.; Campbell, C. T. A Benchmark Database for Adsorption Bond Energies to Transition Metal Surfaces and Comparison to Selected DFT Functionals. *Surf. Sci.* **2015**, *640*, 36−44.
(9) Campbell, C. T.; Sellers, J. R. V. Enthalpies and Entropies of Adsorption on Well-Defined Oxide Surfaces: Experimental Measurements. *Chem. Rev.* **2013**, *113* (6), 4106−4135.
(10) Masuda, T.; Taniguchi, H.; Tsutsumi, K.; Takahashi, H. Direct Measurement of Interaction Energy between Solids and Gases. IV. Acidic and Catalytic Properties of Amorphous and Crystalline AluminoSilicates. *Bull. Chem. Soc. Jpn.* **1979**, *52* (10), 2849−2852.
(11) Auroux, A.; Vedrine, J. C.; Gravelle, P. C. Characterization of Small-Pore Zeolites by Adsorption of Ammonia. In *Studies in Surface Science and Catalysis*; Rouquerol, J., Sing, K. S. W., Eds.; Elsevier, 1982; Vol. *10*, pp 305−322.
(12) Klyachko, A. L. Equation for Differential Heat of Adsorption (DHA) on a Surface with Discrete Nonuniformity. *Kinet. Katal.* **1978**, *19* (5), 1218−1223.
(13) Taylor, H. S. A Theory of the Catalytic Surface. *Proc. R. Soc. London, Ser. A* **1925**, *108* (745), 105−111.
(14) Grasselli, R. K. Site Isolation and Phase Cooperation: Two Important Concepts in Selective Oxidation Catalysis: A Retrospective. *Catal. Today* **2014**, *238*, 10−27.
(15) Schlögl, R. Heterogeneous Catalysis. *Angew. Chem., Int. Ed. Engl.* **2015**, *54* (11), 3465−3520.
(16) Choi, Y. W.; Mistry, H.; Roldan Cuenya, B. New Insights into Working Nanostructured Electrocatalysts through Operando Spectroscopy and Microscopy. *Curr. Opin. Electrochem.* **2017**, *1* (1), 95−103.
(17) Boudart, M. Turnover Rates in Heterogeneous Catalysis. *Chem. Rev.* **1995**, *95* (3), 661−666.
(18) Chen, B. W. J.; Xu, L.; Mavrikakis, M. Computational Methods in Heterogeneous Catalysis. *Chem. Rev.* **2021**, *121* (2), 1007−1048.
(19) Medford, A. J.; Vojvodic, A.; Hummelshøj, J. S.; Voss, J.; Abild-Pedersen, F.; Studt, F.; Bligaard, T.; Nilsson, A.; Nørskov, J. K. From the Sabatier Principle to a Predictive Theory of Transition-Metal Heterogeneous Catalysis. *J. Catal.* **2015**, *328*, 36−42.
(20) Ulissi, Z. W.; Tang, M. T.; Xiao, J.; Liu, X.; Torelli, D. A.; Karamad, M.; Cummins, K.; Hahn, C.; Lewis, N. S.; Jaramillo, T. F.; Chan, K.; Nørskov, J. K. Machine-Learning Methods Enable Exhaustive Searches for Active Bimetallic Facets and Reveal Active Site Motifs for CO_2 Reduction. *ACS Catal.* **2017**, *7* (10), 6600−6608.
(21) Xu, W.; Reuter, K.; Andersen, M. Predicting Binding Motifs of Complex Adsorbates Using Machine Learning with a Physics-Inspired Graph Representation. *Nat. Comput. Sci.* **2022**, *2* (7), 443−450.
(22) Mazheika, A.; Wang, Y.-G.; Valero, R.; Viñes, F.; Illas, F.; Ghiringhelli, L. M.; Levchenko, S. V.; Scheffler, M. Artificial-Intelligence-Driven Discovery of Catalyst Genes with Application to CO_2 Activation on Semiconductor Oxides. *Nat. Commun.* **2022**, *13* (1), 419.
(23) Mallikarjun Sharada, S.; Karlsson, R. K. B.; Maimaiti, Y.; Voss, J.; Bligaard, T. Adsorption on Transition Metal Surfaces: Transferability and Accuracy of DFT Using the ADS41 Dataset. *Phys. Rev. B* **2019**, *100* (3), 035439.
(24) Dietze, E. M.; Gronbeck, H. Ensemble Effects in Adsorbate-Adsorbate Interactions in Microkinetic Modeling. *J. Chem. Theory Comput.* **2023**, *19* (3), 1044−1049.
(25) Reuter, K.; Plaisance, C. P.; Oberhofer, H.; Andersen, M. Perspective: On the Active Site Model in Computational Catalyst Screening. *J. Chem. Phys.* **2017**, *146* (4), 040901.
(26) Pérez-Ramírez, J.; López, N. Strategies to Break Linear Scaling Relationships. *Nat. Catal.* **2019**, *2* (11), 971−976.
(27) Campbell, C. T. Energies of Adsorbed Catalytic Intermediates on Transition Metal Surfaces: Calorimetric Measurements and Benchmarks for Theory. *Acc. Chem. Res.* **2019**, *52* (4), 984−993.
(28) Wernbacher, A. M.; Eichelbaum, M.; Risse, T.; Cap, S.; Trunschke, A.; Schlögl, R. Operando Electrical Conductivity and Complex Permittivity Study on Vanadia Oxidation Catalysts. *J. Phys. Chem. C* **2019**, *123* (13), 8005−8017.
(29) Li, X.; Lunkenbein, T.; Pfeifer, V.; Jastak, M.; Nielsen, P. K.; Girgsdies, F.; Knop-Gericke, A.; Rosowski, F.; Schlögl, R.; Trunschke, A. Selective Alkane Oxidation by Manganese Oxide: Site Isolation of MnO_x Chains at the Surface of $MnWO_4$ Nanorods. *Angew. Chem., Int. Ed. Engl.* **2016**, *55* (12), 4092−4096.
(30) Li, X.; Teschner, D.; Streibel, V.; Lunkenbein, T.; Masliuk, L.; Fu, T.; Wang, Y.; Jones, T.; Seitz, F.; Girgsdies, F.; Rosowski, F.; Schlögl, R.; Trunschke, A. How to Control Selectivity in Alkane Oxidation? *Chem. Sci.* **2019**, *10* (8), 2429−2443.
(31) Eichelbaum, M.; Hävecker, M.; Heine, C.; Karpov, A.; Dobner, C.-K.; Rosowski, F.; Trunschke, A.; Schlögl, R. The Intimate Relationship between Bulk Electronic Conductivity and Selectivity in the Catalytic Oxidation of *n*-Butane. *Angew. Chem., Int. Ed. Engl.* **2012**, *51* (25), 6246−6250.
(32) Koch, G.; Hävecker, M.; Kube, P.; Tarasov, A.; Schlögl, R.; Trunschke, A. The Influence of the Chemical Potential on Defects and Function of Perovskites in Catalysis. *Front. Chem.* **2021**, *9* (775), 746229.
(33) Koch, G.; Hävecker, M.; Teschner, D.; Carey, S. J.; Wang, Y.; Kube, P.; Hetaba, W.; Lunkenbein, T.; Auffermann, G.; Timpe, O.; Rosowski, F.; Schlögl, R.; Trunschke, A. Surface Conditions That Constrain Alkane Oxidation on Perovskites. *ACS Catal.* **2020**, *10* (13), 7007−7020.
(34) Trunschke, A.; Noack, J.; Trojanov, S.; Girgsdies, F.; Lunkenbein, T.; Pfeifer, V.; Hävecker, M.; Kube, P.; Sprung, C.; Rosowski, F.; Schlögl, R. The Impact of the Bulk Structure on Surface Dynamics of Complex Mo−V-based Oxide Catalysts. *ACS Catal.* **2017**, *7* (4), 3061−3071.
(35) Wernbacher, A. M.; Kube, P.; Hävecker, M.; Schlögl, R.; Trunschke, A. Electronic and Dielectric Properties of MoV-Oxide (M1 Phase) under Alkane Oxidation Conditions. *J. Phys. Chem. C* **2019**, *123* (21), 13269−13282.
(36) Foppa, L.; Ghiringhelli, L. M.; Girgsdies, F.; Hashagen, M.; Kube, P.; Hävecker, M.; Carey, S. J.; Tarasov, A.; Kraus, P.; Rosowski, F.; Schlögl, R.; Trunschke, A.; Scheffler, M. Materials Genes of Heterogeneous Catalysis from Clean Experiments and Artificial Intelligence. *MRS Bull.* **2021**, *46* (11), 1016−1026.
(37) Foppa, L.; Rüther, F.; Geske, M.; Koch, G.; Girgsdies, F.; Kube, P.; Carey, S. J.; Hävecker, M.; Timpe, O.; Tarasov, A. V.; Scheffler, M.; Rosowski, F.; Schlögl, R.; Trunschke, A. Data-Centric Heterogeneous Catalysis: Identifying Rules and Materials Genes of Alkane Selective Oxidation. *J. Am. Chem. Soc.* **2023**, *145* (6), 3427−3442.
(38) Grant, J. T.; Venegas, J. M.; McDermott, W. P.; Hermans, I. Aerobic Oxidations of Light Alkanes over Solid Metal Oxide Catalysts. *Chem. Rev.* **2018**, *118* (5), 2769−2815.
(39) Védrine, J. C. Metal Oxides in Heterogeneous Oxidation Catalysis: State of the Art and Challenges for a More Sustainable World. *ChemSusChem* **2019**, *12* (3), 577−588.
(40) Dummer, N. F.; Bartley, J. K.; Hutchings, G. J. Vanadium Phosphate Materials as Selective Oxidation Catalysts. In *Advances in Catalysis*; Gates, B. C., Knözinger, H., Eds.; Elsevier Academic Press Inc: San Diego, 2011; Vol. *54*, pp 189−247.
(41) Masliuk, L.; Schmidt, F.-P.; Hetaba, W.; Plodinec, M.; Auffermann, G.; Hermann, K.; Teschner, D.; Girgsdies, F.; Trunschke, A.; Schlögl, R.; Lunkenbein, T. Compositional Decou-

https://doi.org/10.1021/acscatal.4c01308
ACS Catal. 2024, 14, 12581−12591

pling of Bulk and Surface in Open-Structured Complex Mixed Oxides. *J. Phys. Chem. C* **2020**, *124* (42), 23069−23077.
(42) Jozefowicz, L. C.; Karge, H. G.; Coker, E. N. Microcalorimetric Investigation of H-ZSM-5 Zeolites Using an Ultrahigh-Vacuum System for Gas Adsorption. *J. Phys. Chem.* **1994**, *98* (33), 8053−8060.
(43) Wrabetz, S.; Yang, X.; Tzolova-Müller, G.; Schlögl, R.; Jentoft, F. C. Characterization of Catalysts in their Active State by Adsorption Microcalorimetry: Experimental Design and Application to Sulfated Zirconia. *J. Catal.* **2010**, *269* (2), 351−358.
(44) Auroux, A. *Calorimetry and Thermal Methods in Catalysis*; Springer: Berlin, Heidelberg, 2013.
(45) Kube, P.; Frank, B.; Schlögl, R.; Trunschke, A. Isotope Studies in Oxidation of Propane over Vanadium Oxide. *ChemCatChem* **2017**, *9* (18), 3446−3455.
(46) Hävecker, M.; Wrabetz, S.; Kröhnert, J.; Csepei, L.-I.; Naumann d'Alnoncourt, R.; Kolen'ko, Y. V.; Girgsdies, F.; Schlögl, R.; Trunschke, A. Surface Chemistry of Phase-Pure M1 MoVTeNb Oxide During Operation in Selective Oxidation of Propane to Acrylic Acid. *J. Catal.* **2012**, *285* (1), 48−60.
(47) Kube, P.; Frank, B.; Wrabetz, S.; Kröhnert, J.; Hävecker, M.; Velasco-Vélez, J.; Noack, J.; Schlögl, R.; Trunschke, A. Functional Analysis of Catalysts for Lower Alkane Oxidation. *ChemCatChem* **2017**, *9* (4), 573−585.
(48) Klumpers, B.; Hensen, E. J. M.; Filot, I. A. W. Lateral Interactions of Dynamic Adlayer Structures from Artificial Neural Networks. *J. Phys. Chem. C* **2022**, *126* (12), 5529−5540.
(49) Eder, F.; Lercher, J. A. On the Role of the Pore Size and Tortuosity for Sorption of Alkanes in Molecular Sieves. *J. Phys. Chem. B* **1997**, *101* (8), 1273−1278.
(50) Zhao, R.; Khare, R.; Zhang, Y.; Sanchez-Sanchez, M.; Bermejo-Deval, R.; Liu, Y.; Lercher, J. A. Promotion of Adsorptive and Catalytic Properties of Zeolitic Brønsted Acid Sites by Proximal Extra-Framework $Si(OH)_x$ Groups. *Nat. Catal.* **2023**, *6* (1), 68−79.
(51) Kämper, A.; Auroux, A.; Baerns, M. A Molecular Mechanics Study of the Adsorption of Ethane and Propane on a $V_2O_5(001)$ Surface. *Phys. Chem. Chem. Phys.* **2000**, *2* (5), 1069−1075.
(52) Alexopoulos, K.; Reyniers, M.-F.; Marin, G. B. Reaction Path Analysis of Propene Selective Oxidation over V_2O_5 and V_2O_5/TiO_2. *J. Catal.* **2012**, *295* (0), 195−206.
(53) Fu, H.; Liu, Z.-P.; Li, Z.-H.; Wang, W.-N.; Fan, K.-N. Periodic Density Functional Theory Study of Propane Oxidative Dehydrogenation over $V_2O_5(001)$ Surface. *J. Am. Chem. Soc.* **2006**, *128* (34), 11114−11123.
(54) Licht, R. B.; Getsoian, A. B.; Bell, A. T. Identifying the Unique Properties of α-$Bi_2Mo_3O_{12}$ for the Activation of Propene. *J. Phys. Chem. C* **2016**, *120* (51), 29233−29247.
(55) Pudar, S.; Oxgaard, J.; Chenoweth, K.; van Duin, A. C. T.; Goddard, W. A. Mechanism of Selective Oxidation of Propene to Acrolein on Bismuth Molybdates from Quantum Mechanical Calculations. *J. Phys. Chem. C* **2007**, *111* (44), 16405−16415.
(56) Shee, D.; Deo, G. In Situ DRIFT Studies of Alkane Adsorption on Vanadia Supported Titania-Doped Catalysts. *Catal. Today* **2019**, *325*, 25−32.
(57) Krauß, K.; Drochner, A.; Fehlings, M.; Kunert, J.; Vogel, H. Characterisation of the Structure of Adsorbates: An In Situ DRIFTS-Study of the Partial Oxidation of Unsaturated Aldehydes on Mo/V Oxide Catalysts. *J. Mol. Catal. A: Chem.* **2000**, *162* (1), 413−422.
(58) Batiot, C.; Hodnett, B. K. The Role of Reactant and Product Bond Energies in Determining Limitations to Selective Catalytic Oxidations. *Appl. Catal., A* **1996**, *137* (1), 179−191.
(59) *CRC Handbook of Chemistry and Physics*; Rumble, J. R., Ed. 103rd ed.; Taylor&Francis Group, 2022.
(60) Vogt, C.; Weckhuysen, B. M. The Concept of Active Site in Heterogeneous Catalysis. *Nat. Rev. Chem* **2022**, *6* (2), 89−111.
(61) van Santen, R. A. Physical Chemistry, Elementary Kinetics. In *Modern Heterogeneous Catalysis*; Santen, R. A., Ed.; Wiley Online Library, 2017; pp 59−116.
(62) Nørskov, J. K.; Bligaard, T.; Logadottir, A.; Bahn, S.; Hansen, L. B.; Bollinger, M.; Bengaard, H.; Hammer, B.; Sljivancanin, Z.; Mavrikakis, M.; Xu, Y.; Dahl, S.; Jacobsen, C. J. H. Universality in Heterogeneous Catalysis. *J. Catal.* **2002**, *209* (2), 275−278.
(63) Lei, Y.; Yan, M. DFT Studies of Selective Oxidation of Propene on the $MoO_3(010)$ Surface. *Phys. Chem. Chem. Phys.* **2021**, *23* (4), 2792−2804.
(64) Liu, J.; Mohamed, F.; Sauer, J. Selective Oxidation of Propene by Vanadium Oxide Monomers Supported on Silica. *J. Catal.* **2014**, *317*, 75−82.
(65) Heenemann, M.; Heine, C.; Hävecker, M.; Trunschke, A.; Schlögl, R. Influence of Steam on a Vanadyl Pyrophosphate Catalyst During Propane Oxidation. *J. Phys. Chem. B* **2018**, *122* (2), 695−704.
(66) Caldarelli, A.; Bañares, M. A.; Cortelli, C.; Luciani, S.; Cavani, F. An Investigation on Surface Reactivity of Nb-doped Vanadyl Pyrophosphate Catalysts by Reactivity Experiments and In Situ Raman Spectroscopy. *Catal. Sci. Technol.* **2014**, *4* (2), 419−427.
(67) Ivars-Barceló, F.; Hutchings, G. J.; Bartley, J. K.; Taylor, S. H.; Sutter, P.; Amorós, P.; Sanchis, R.; Solsona, B. Relationship between Bulk Phase, Near Surface and Outermost Atomic Layer of VPO Catalysts and their Catalytic Performance in the Oxidative Dehydrogenation of Ethane. *J. Catal.* **2017**, *354*, 236−249.
(68) Erdem, E.; Tarasov, A. V.; Kube, P.; Koch, G.; Plodinec, M.; Lunkenbein, T.; Carey, S.; Wang, Y.; Hävecker, M.; Rosowski, F.; Schlögl, R.; Trunschke, A. The Influence of Melting on Catalysis in Propane Oxidation. *ChemCatChem* **2024**, *16* (3), No. e202301242.
(69) Vogt, C.; Monai, M.; Sterk, E. B.; Palle, J.; Melcherts, A. E. M.; Zijlstra, B.; Groeneveld, E.; Berben, P. H.; Boereboom, J. M.; Hensen, E. J. M.; Meirer, F.; Filot, I. A. W.; Weckhuysen, B. M. Understanding Carbon Dioxide Activation and Carbon−Carbon Coupling over Nickel. *Nat. Commun.* **2019**, *10* (1), 5330.
(70) Vogt, C.; Groeneveld, E.; Kamsma, G.; Nachtegaal, M.; Lu, L.; Kiely, C. J.; Berben, P. H.; Meirer, F.; Weckhuysen, B. M. Unravelling Structure Sensitivity in CO_2 Hydrogenation over Nickel. *Nat. Catal.* **2018**, *1* (2), 127−134.
(71) Klag, L.; Sheppard, T. L.; Grunwaldt, J.-D. An Advanced Characterization Toolbox for Selective Olefin Oxidation Catalysts. *ChemCatChem* **2023**, *15* (3), No. e202201276.
(72) Marshall, C. P.; Schumann, J.; Trunschke, A. Achieving Digital Catalysis: Strategies for Data Acquisition, Storage and Use. *Angew. Chem., Int. Ed. Engl.* **2023**, *62* (30), No. e202302971.

https://doi.org/10.1021/acscatal.4c01308
ACS Catal. 2024, 14, 12581−12591